

# Confined Quasiparticle Dynamics in Long-Range Interacting Quantum Spin Chains

Fangli Liu,<sup>1</sup> Rex Lundgren,<sup>1</sup> Paraj Titum,<sup>1,2</sup> Guido Pagano,<sup>1</sup> Jiehang Zhang,<sup>1</sup>  
Christopher Monroe,<sup>1,2</sup> and Alexey V. Gorshkov<sup>1,2</sup>

<sup>1</sup>*Joint Quantum Institute, NIST/University of Maryland, College Park, MD 20742, USA*

<sup>2</sup>*Joint Center for Quantum Information and Computer Science,  
NIST/University of Maryland, College Park, MD 20742, USA*

We study the quasiparticle excitation and quench dynamics of the one-dimensional transverse-field Ising model with power-law ( $1/r^\alpha$ ) interactions. We find that long-range interactions give rise to a confining potential, which couples pairs of domain walls (kinks) into bound quasiparticles, analogous to mesonic bound states in high-energy physics. We show that these quasiparticles have signatures in the dynamics of order parameters following a global quench and the Fourier spectrum of these order parameters can be exploited as a direct probe of the masses of the confined quasiparticles. We introduce a two-kink model to qualitatively explain the phenomenon of long-range-interaction-induced confinement, and to quantitatively predict the masses of the bound quasiparticles. Furthermore, we illustrate that these quasiparticle states can lead to slow thermalization of one-point observables for certain initial states. Our work is readily applicable to current trapped-ion experiments.

Long-range interacting quantum systems occur naturally in numerous quantum simulators [1–10]. A paradigmatic model considers interactions decaying with distance  $r$  as a power law  $1/r^\alpha$ . This describes the interaction term in trapped-ion spin systems [3, 11–15], polar molecules [16–19], magnetic atoms [5, 20, 21], and Rydberg atoms [1, 2, 22, 23]. One remarkable consequence of long-range interactions is the breakdown of locality, where quantum information, bounded by linear ‘light cones’ in short-range interacting systems [24], can propagate super-ballistically or even instantaneously [25–30]. Lieb-Robinson linear light cones have been generalized to logarithmic and polynomial light cones for long-range interacting systems [25, 26, 31], and non-local propagation of quantum correlations in one-dimensional (1D) spin chains has been observed in trapped-ion experiments [12, 13]. Moreover, 1D long-range interacting quantum spin chains can host novel physics that is absent in their short-range counterparts, such as continuous symmetry breaking [32, 33].

More recently, it has been shown that confinement—which has origins in high-energy physics—has dramatic signatures in the quantum quench dynamics of short-range interacting spin chains [34]. Owing to confinement, quarks cannot be directly observed in nature as they form mesons and baryons due to strong interactions [35, 36]. An archetypal model with analogous confinement effects in quantum many-body systems is the 1D short-range interacting Ising model with both transverse and longitudinal fields [37–42]. For a vanishing longitudinal field, domain-wall quasiparticles propagate freely and map out light-cone spreading of quantum information [41–44]. As first proposed by McCoy and Wu [45–47], a non-zero longitudinal field induces an attractive linear potential between two domain walls and confines them into mesonic bound quasiparticles. Recently, Kormos et al. investigated the effect of these bound states on quench dynamics and showed that the non-equilibrium dynamics can be used to probe confinement [34].

In this work, we study the non-equilibrium dynamics of the long-range interacting transverse-field Ising model *without a longitudinal field* after a global quantum quench. We find that

long-range interactions introduce an effective attractive force between a pair of domain walls, thus confining them into a bound state, analogous to the meson in high-energy physics. We calculate time-dependent order parameters and connected correlation functions, both of which feature clear signatures of bound quasiparticle excitations [41, 42]. The masses of these bound quasiparticles—the energy gaps relative to the ground state—can be directly extracted from the Fourier spectrum of time-dependent order parameters [34, 41, 42]. We introduce a two-kink model, i.e. we restrict spin configurations to states with only a pair of domain walls (kinks), to explicitly show that the confining potential comes from long-range interactions. The two-kink model also gives good predictions for the quasiparticles’ masses and their dispersion relations. Furthermore, we study the effect of confined quasiparticles on the thermalization of different initial states [41, 42]. We find that for certain initial states, one-point observables exhibit slow thermalization [41, 42, 48, 49], which might help protect ordered phases in the prethermal region [50–52].

We note that our study is in agreement with the general mechanism of global quantum quenches, first formulated in Refs. [41, 42, 44] for short-range interacting systems, and demonstrates that the general theory developed in Refs. [41, 42, 44] holds for systems with long-range interactions. Our work is well within the reach of current trapped-ion experiments [15] and other atomic, molecular, and optical (AMO) experimental platforms [1, 9, 53].

*The model.*— Let us consider a quantum spin chain with long-range interactions, described by the following Hamiltonian,

$$H = - \sum_{i < j}^L \frac{J}{r_{ij}^\alpha} \sigma_i^z \sigma_j^z - B \sum_{i=1}^L \sigma_i^x, \quad (1)$$

where  $\sigma_i^\mu$  are the Pauli matrices on site  $i$ ,  $L$  is the system size,  $r_{ij}$  is the distance between sites  $i$  and  $j$  (nearest-neighbor spacing is assumed to be equal to 1),  $J$  sets the overall energy scale (taken to be 1 without loss of generality),  $B$  is a global transverse magnetic field, and  $\alpha$  describes the power-law de-

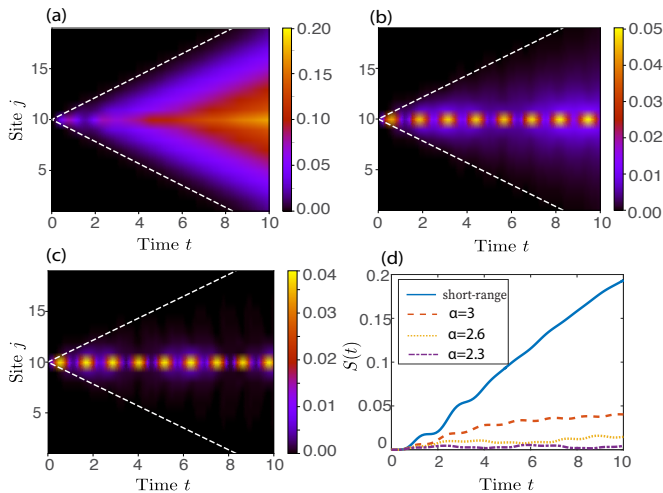


FIG. 1. (color online) (a)-(c)  $\langle \sigma_j^z \sigma_k^z \rangle_c$ , and (d)  $S_A(t)$  versus  $t$  after a quantum quench with initial state  $|\Psi_0\rangle$ .  $L = 19$ ,  $k = 10$ , and  $B = 0.27$ . (a) Short-range interacting case ( $\alpha \rightarrow \infty$ ), (b)  $\alpha = 2.6$ , (c)  $\alpha = 2.3$ . The dashed white lines illustrate the maximal velocity,  $4B$ , of freely propagating domain walls in the short-range interacting case [34]. (d)  $S_A(t)$  for various  $\alpha$ .

cay of long-range interactions. In this work, we consider periodic boundary conditions unless otherwise specified ( $r_{ij}$  is then the shortest distance between sites  $i$  and  $j$ ).

In the nearest-neighbor interacting limit ( $\alpha \rightarrow \infty$ ),  $H$  is exactly solvable via a Jordan-Wigner mapping to spinless fermions. It exhibits a second-order phase transition at  $B = 1$ , which separates the ferromagnetic and paramagnetic phases [54]. The phase transition persists if one turns on long-range interactions; however, the critical value of  $B$  increases [55–58]. In trapped-ion experiments, the range of the power-law exponent can be tuned within  $0 < \alpha < 3$  by changing the detuning of the applied optical fields from phonon sidebands. We restrict the numerics to  $\alpha > 1$  in order to ensure a well-behaved thermodynamic limit (the case of  $\alpha \in [0, 1]$  will be briefly discussed later). Several experiments have investigated the real-time dynamics of the above model (or closely related models), including dynamical phase transitions [15, 59], the non-local propagation of correlations [12, 13], the time-crystal phase [50], and many-body localization [14].

*Quench dynamics.*— Let us first study the quench dynamics of the above model. We focus on a simple initial state with all spins polarized in the  $z$  direction,  $|\Psi_0\rangle = |\dots \uparrow \uparrow \uparrow \dots\rangle$ , which can be easily prepared in trapped-ion experiments [15]. The system is allowed to evolve under the Hamiltonian (1). This is equivalent to a global quantum quench from zero to finite  $B$  [15, 41, 42]. In order to explore the physics of domain walls, we focus on quantum quenches within the ferromagnetic phase [43, 60]. Finally, while we have chosen a spin-polarized initial state, confinement persists when the initial state is chosen as the ground state of Eq. (1) with  $B$  in the ferromagnetic region.

We use the Krylov-space method to simulate the quench

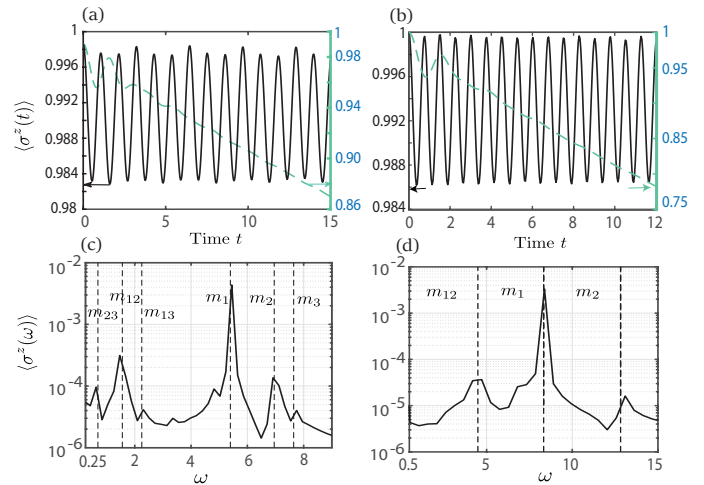


FIG. 2. (color online) (a)-(b)  $\langle \sigma^z(t) \rangle$  (black line) versus time after quenching to (a)  $\alpha = 2.3$ ,  $B = 0.27$ , (b)  $\alpha = 1.4$ ,  $B = 0.35$  for  $L = 20$ . The dashed green lines show the decay of  $\langle \sigma^z(t) \rangle$  for the short-range model with the same  $B$ . (c)-(d) Fourier spectrum of  $\langle \sigma^z(t) \rangle$  for the long-range case in (a) and (b), respectively. The largest time for the Fourier transform is up to  $t = 30$  and  $12$  for (c) and (d), respectively. The parameters in (b,d) are accessible in current trapped-ion experiments [15]. The dashed lines show the mesonic masses ( $m_i$ ) and their differences ( $m_{ij} \equiv m_j - m_i$ ) calculated using the two-kink model.

dynamics of our system [61, 62]. Figs. 1(a)-(c) show the equal-time connected correlation functions,  $\langle \sigma_j^z(t) \sigma_k^z(t) \rangle_c = \langle \sigma_j^z(t) \sigma_k^z(t) \rangle - \langle \sigma_j^z(t) \rangle \langle \sigma_k^z(t) \rangle$ , after the sudden quench (we take  $k$  to be the central lattice site). In the short-range interacting limit [Fig. 1(a)], we recover the exactly solvable case, where correlations spread with a velocity ( $4B$ ) equal to twice the maximal speed of free domain-walls [34, 43, 44]. Increasing the Ising interaction range (decreasing  $\alpha$ ) strongly suppresses the magnitude of  $\langle \sigma_j^z(t) \sigma_k^z(t) \rangle_c$ , as shown in Figs. 1(b) and 1(c). One can also see the oscillatory behaviour of correlations in Figs. 1(b) and 1(c), similar to that of Ref. [34]. However, we emphasize that the light-cone spreading of correlations is always present [34, 44], though it may have a different velocity depending on the quasiparticles in the system [44]. The actual extent of the light cone becomes clearer by zooming in on the ‘black’ regions of Figs. 1(b) and 1(c) (see Supplemental Material for details [63]). This result is in agreement with the general mechanism of global quantum quenches first derived in Ref. [44].

The propagating quasiparticles produced by the quench map out the light-cone spreading of correlations [44, 63] and also lead to the growth of entanglement entropy [34]. In Fig. 1(d), we plot the growth of entanglement entropy,  $S_A(t) = -\text{Tr}[\rho_A(t) \ln(\rho_A(t))]$ , where  $\rho_A(t)$  is the reduced density matrix of one half of the chain, for various  $\alpha$ . As one can see, the entanglement entropy growth for smaller  $\alpha$  is much slower than the short-range case (linear growth). This is because there are less propagating quasiparticles for longer-range interactions, i.e. most quasiparticles produced by the

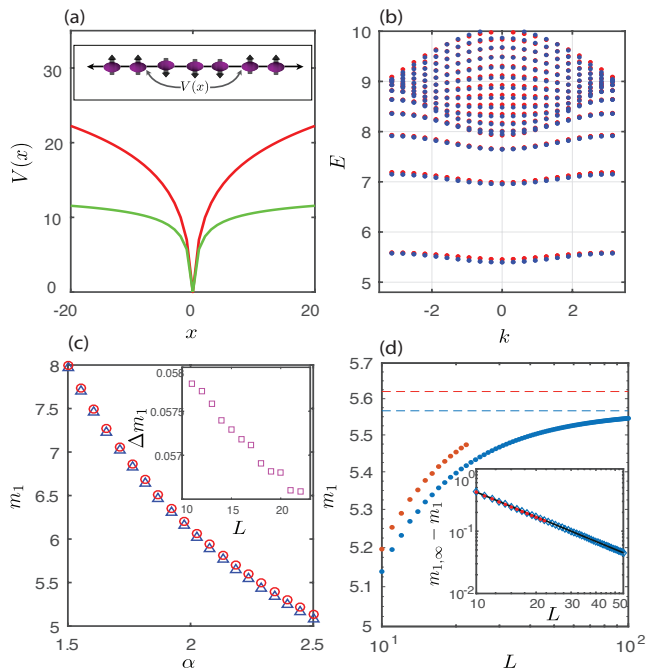


FIG. 3. (color online) (a) Potential energy as a function of distance  $x$  between the two domain walls ( $n = |x|$ ). Red line:  $\alpha = 1.9$ ; green line:  $\alpha = 2.3$ . Inset: typical spin configuration of two-domain-wall states. (b)-(d) Comparison of two-kink model (blue markers) and ED results (red markers) (b) Energy spectrum. Parameters:  $\alpha = 2.3$ ,  $B = 0.27$ ,  $L = 20$ . (c)  $m_1$  versus  $\alpha$  with parameters  $B = 0.27$  and  $L = 22$ . Inset: Difference of  $m_1$  between the two methods,  $\Delta m_1$ , versus  $L$ . (d)  $m_1$  versus  $L$ , with the same parameters as in (b). The dashed lines are  $m_{1,\infty}$ . The inset shows  $m_{1,\infty} - m_1$  versus system size. The black line shows the fitting of the two-kink model's data to  $(1/L)^\beta$ , with  $\beta = 1.315$ . ED data has similar scaling with  $\beta = 1.34$ .  $m_{1,\infty}$  is chosen as 5.56 (5.62) for the two-kink model (ED).

quench have zero momentum [34].

We plot time-dependent order parameters  $\langle \sigma^z(t) \rangle = \frac{1}{L} \sum_i \langle \sigma_i^z(t) \rangle$  in Figs. 2(a) and (b) [64]. Different from the rapid exponential decay of the magnetization for the short-range case,  $\langle \sigma^z(t) \rangle$  exhibits periodic oscillations with almost no decay [41, 42, 65–67] in the time window we are showing. We emphasize that the qualitative change in dynamics is caused by the long-range interactions, not by an additional longitudinal field as in the short-range interacting case [34, 41, 42]. The Fourier spectrum [68] of  $\langle \sigma^z(t) \rangle$  illustrates that the oscillations are associated with multiple different frequencies (Figs. 2(c) and 2(d)). As we will see, these frequencies are in good agreement with the masses (and their differences) of quasiparticles [41, 42].

*Two-kink model and bound states.*— To understand the quasiparticles in our system, we use a two-kink model to perturbatively study the low-energy excitations of Eq. (1). The two-kink model has been used to phenomenologically study the confinement of excitations in short-range interacting quasi-1D compounds [37, 69]. The idea is to restrict

the Hilbert-space to two domain-wall states [see inset of Fig. 3(a)], where regions of different magnetization are separated by the two domain walls. The projected model is expected to work well when  $B$  is much smaller than  $J$ [34].

The Hilbert space of the projected model is spanned by states of  $n$  down-spins (clustered together) which we represent as:  $|j, n\rangle = |\dots \uparrow \uparrow \downarrow_j \downarrow \dots \downarrow \downarrow_{(j+n-1)} \uparrow \uparrow \dots\rangle$ , where  $j$  is the starting position of the cluster. The projected Hamiltonian,  $\mathcal{H} = \mathcal{P}H\mathcal{P}$ , where  $\mathcal{P}$  is the projection operator to the two-domain-wall subspace, acts on  $|j, n\rangle$  as follows,

$$\mathcal{H}|j, n\rangle = V(n)|j, n\rangle - B[|j, n+1\rangle + |j, n-1\rangle + |j+1, n+1\rangle + |j-1, n+1\rangle]. \quad (2)$$

Here, we have defined the potential energy as  $V(n) = \langle j, n|\mathcal{H}|j, n\rangle - \langle \Psi_0|\mathcal{H}|\Psi_0\rangle$ . For our translational invariant system, the momentum  $k$  is a good quantum number, and  $\mathcal{H}$  is diagonal in the momentum basis. Fourier transforming the two-domain-wall state,  $|k, n\rangle = \frac{1}{\sqrt{L}} \sum_{j=1}^L \exp(-ikj - ikn/2)|j, n\rangle$ , gives

$$\mathcal{H} = \sum_{k,n} V(n)|k, n\rangle \langle k, n| - 2B \cos \frac{k}{2} |k, n\rangle \langle k, n+1| - 2B \cos \frac{k}{2} |k, n\rangle \langle k, n-1|. \quad (3)$$

For an infinitely large system, the potential energy of a two-domain-wall spin configuration is

$$V(n) = 4n\zeta(\alpha)J - 4J \sum_{1 \leq l < n} \sum_{1 \leq r \leq l} \frac{1}{r^\alpha}, \quad (4)$$

where  $\zeta(\alpha) = \sum_{z=1}^{\infty} \frac{1}{z^\alpha}$  denotes the Riemann zeta function. As plotted in Fig. 3(a),  $V(n)$  increases with the distance between domain walls. For the short-range model studied by Kormos *et al.* [34], the confining potential is due to an additional on-site longitudinal magnetic field. In our case, the confining potential is intrinsically generated by the long-range interactions.

The picture now becomes clear: the long-range Ising interaction gives rise to an effective potential, which increases with separation between domain walls, while the transverse magnetic field acts as kinetic energy for the two domain walls (increasing or decreasing the size of the cluster). Therefore, a pair of domain walls, each of which is free quasiparticle in the short-range interacting limit, become bounded together when  $\alpha$  decreases. Note that  $V(n)$  has an upper bound when  $\alpha > 2$ , as illustrated in Fig. 3(a) (see Supplemental Material [63]). This indicates that the lower part of the energy spectrum [obtained by diagonalizing Eq. (3)] is composed of domain-wall bound states, while above some energy threshold, we have a continuum of states [Fig. 3(b)]. For  $\alpha \leq 2$ , however, all excitations within the two-kink model are bound quasiparticles, as the confining potential  $V(n)$  become unbounded when  $n \rightarrow \infty$  [63]. This is in contrast with finite-range interacting models, where the potential becomes flat for  $n$  greater than the

interaction range. In other words, for finite-range interacting systems two domain walls will behave like freely propagating particles if the domain size of the initial state exceeds the interaction range.

Fig. 3(b) shows the energy spectrum calculated by the two-kink model (blue dots) and exact diagonalization (ED) of the full Hilbert space (red dots). As one can see, the energy spectrum agrees well for the two methods, demonstrating that low-energy excitations are dominated by two-domain-wall states. The bound states' masses [70] and dispersion relations can be simply read out from the energy spectrum. Moreover, the Fourier frequencies of  $\langle \sigma^z(t) \rangle$  [Figs. 2(c) and 2(d)] are compatible, to high accuracy, with the masses of the bound states (and their differences) calculated using the two-kink model [41, 42]. This demonstrates that the quench dynamics of the long-range interacting model is indeed dominated by confined domain walls.

We compare the smallest bound state mass,  $m_1$ , as a function of  $\alpha$  calculated using the two-kink model (blue) and ED (red) in Fig. 3(c). For a large range of  $\alpha$ , we see excellent agreement between the two methods, and the numerical difference does not increase for larger  $L$  [inset of Fig. 3(c)]. The masses increase with  $L$  as longer chains have more interaction terms [63]. However,  $V(n)$  is finite (for finite  $n$ ) in the thermodynamic limit, since the Riemann zeta function converges for  $\alpha > 1$  [71]. This leads to finite masses, even for an infinite system when  $\alpha > 1$  (see Supplemental Material [63]). Fig. 3(d) shows the system-size dependence of  $m_1$ . The mass calculated from the two-kink model indeed exhibits convergence in the thermodynamic limit. For the two-kink model, the difference between  $m_1$  and its thermodynamic value,  $m_{1,\infty}$ , scales as  $(1/L)^\beta$ , with  $\beta \approx \alpha - 1$  [63], as shown in the inset. While we cannot verify convergence using ED, we do observe similar scaling of  $m_1$  [inset of Fig. 3(d)]. For  $0 \leq \alpha \leq 1$ ,  $V(n)$  becomes infinite, even for finite  $n$ , and thus the bound states have infinite energy (as the Riemann zeta function diverges for  $0 \leq \alpha \leq 1$  [71]), consistent with the results of Ref. [72].

*Strong and weak thermalization.*— For the quenches we have considered, both the order parameter decay and entanglement entropy growth are quite slow (Fig. 1). This motivates us to study thermalization in our long-range model. Previous studies of the short-range Ising model have observed rapid (strong) or slow (weak) thermalization of one-point functions for different initial states [41, 42, 48, 49, 73–76]. As first shown in Ref. [41], undamped oscillations (weak thermalization) of one-point observable occurs within an intermediate time window when the matrix element between the initial state and the quasiparticle state of the quench operator and of the observable are both non-zero [41, 42]. Rapid decay occurs when this condition is not satisfied. Numerical results consistent with this finding have been observed in Refs. [34, 42, 48, 49, 75]. Here, we illustrate that these two distinct thermalization behaviors also occur in the long-range Ising model and that slow thermalization can arise when the quasi-

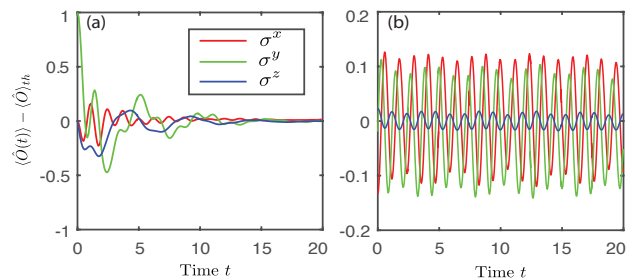


FIG. 4. (color online) Strong (a) and weak (b) thermalization for different initial states. (a)  $\langle \sigma^\mu(t) \rangle - \langle \sigma^\mu \rangle_{\text{th}}$  for initial state  $|Y_+\rangle$ .  $\langle \sigma^\mu(t) \rangle$  rapidly converges to its thermal value. (b) Same as (a), but for initial state  $|Z_+\rangle$ . The observables show strong oscillatory behavior. Parameters:  $\alpha = 2.3$ ,  $B = 0.37$ ,  $L = 20$ .

particles are the result of confinement [34, 42, 75].

In order to see this, we consider the time evolution of two different initial states (with the same quenched Hamiltonian):  $|Z_+\rangle = \prod_j |\uparrow_j\rangle$  (the same state considered before) and  $|Y_+\rangle = \prod_j \frac{1}{\sqrt{2}}(|\uparrow_j\rangle + i|\downarrow_j\rangle)$  [48]. For  $|Z_+\rangle$ , the quenched operator has the same parity as the two-kink bound state and thus the matrix elements mentioned above have non-zero values [41, 42]. We therefore expect slow dynamics with oscillations due to the bound quasiparticles [41, 42]. On the other hand,  $|Y_+\rangle$  does not satisfy this condition which suggests rapid thermalization.

We calculate the difference between the time-dependent expectation value of single-body observables,  $\langle \sigma^\mu(t) \rangle$ , and their thermal expectation value,  $\langle \sigma^\mu \rangle_{\text{th}} = \text{tr}(e^{-\beta_\Psi H} \sigma^\mu) / \text{tr}(e^{-\beta_\Psi H})$ , where the temperature,  $\frac{1}{\beta_\Psi}$ , is determined by (see for example, [77]):

$$\frac{\langle \Psi | H | \Psi \rangle}{\langle \Psi | \Psi \rangle} = \frac{\text{tr}(H e^{-\beta_\Psi H})}{\text{tr}(e^{-\beta_\Psi H})}. \quad (5)$$

Here,  $|\Psi\rangle$  denotes the initial state. As illustrated in Fig. 4(a), for  $|Y_+\rangle$ , all single-body observables converge to  $\langle \sigma^\mu \rangle_{\text{th}}$  rapidly, indicating strong thermalization, as expected. For  $|Z_+\rangle$ , we instead observe strong oscillatory behavior [41, 42], with Fourier frequencies consistent with the masses of the bound quasiparticles, around  $\langle \sigma^\mu \rangle_{\text{th}}$  [Fig. 4(b)]. Within the time window shown, we observe almost no decay of these observables, indicating much slower thermalization compared to  $|Y_+\rangle$  [48, 49].

*Conclusions and outlook.*— We have found that the low-energy excitations of the long-range transverse-field Ising model are confined domain-walls. These bound quasiparticles, which arise due to long-range interactions, have clear signatures in the quench dynamics of the system [34, 41, 42, 44]. Furthermore, our work shows that general quantum mechanisms of quench dynamics developed for short-range interacting systems [41, 42, 44] hold for long-range interacting systems. These results can be readily investigated in current trapped ion experiments [15] and other AMO system with long-range interaction [1, 9, 53]. The slow thermalization



[41, 42] of one-point functions induced by long-range interactions has potential applications for stabilizing non-equilibrium phases of matter in the prethermal region, such as time-crystals [50–52] and Floquet symmetry-protected topological phases of matter [78–82]. Finally, it would be interesting to study the effects of long-range interactions on quench dynamics of  $q$ -state Potts models, which admit mesonic, as well as baryonic excitations [83–86].

We are grateful to F. Verstraete, P. Calabrese, A. Bapat, J. Garrison, S.K. Chu, C. Flower, and S. Whitsitt for useful discussions. F.L., R.L., and A.V.G. acknowledge support by ARO, NSF Ideas Lab on Quantum Computing, the DoE ASCR Quantum Testbed Pathfinder program, ARL CDQI, NSF PFC at JQI, and ARO MURI. R.L. and P.T. were supported by NIST NRC Research Postdoctoral Associateship Awards. G.P., J.Z. and C.M. are supported by the ARO and AFOSR Atomic and Molecular Physics Programs, the AFOSR MURI on Quantum Measurement and Verification, the IARPA LogiQ program, and the NSF Physics Frontier Center at JQI. This research was supported in part by the National Science Foundation under Grant No. NSF PHY-1748958.

- 
- [1] M. Saffman, T. G. Walker, and K. Mølmer, “Quantum information with rydberg atoms,” *Rev. Mod. Phys.* **82**, 2313 (2010).
- [2] P. Schauß, M. Cheneau, M. Endres, T. Fukuhara, S. Hild, A. Omran, T. Pohl, C. Gross, S. Kuhr, and I. Bloch, “Observation of spatially ordered structures in a two-dimensional Rydberg gas,” *Nature (London)* **491**, 87 (2012).
- [3] R. Islam, C. Senko, W. C. Campbell, S. Korenblit, J. Smith, A. Lee, E. E. Edwards, C.-C. J. Wang, J. K. Freericks, and C. Monroe, “Emergence and Frustration of Magnetism with Variable-Range Interactions in a Quantum Simulator,” *Science* **340**, 583 (2013).
- [4] F. Dolde, I. Jakobi, B. Naydenov, N. Zhao, S. Pezzagna, C. Trautmann, J. Meijer, P. Neumann, F. Jelezko, and J. Wrachtrup, “Room-temperature entanglement between single defect spins in diamond,” *Nat. Phys.* **9**, 139 (2013).
- [5] M. Lu, N. Q. Burdick, and B. L. Lev, “Quantum degenerate dipolar fermi gas,” *Phys. Rev. Lett.* **108**, 215301 (2012).
- [6] L. Childress, M. V. G. Dutt, J. M. Taylor, A. S. Zibrov, F. Jelezko, J. Wrachtrup, P. R. Hemmer, and M. D. Lukin, “Coherent Dynamics of Coupled Electron and Nuclear Spin Qubits in Diamond,” *Science* **314**, 281 (2006).
- [7] J. R. Weber, W. F. Koehl, J. B. Varley, A. Janotti, B. B. Buckley, C. G. Van de Walle, and D. D. Awschalom, “Quantum computing with defects,” *Proc. Natl. Acad. Sci. U.S.A.* **107**, 8513 (2010).
- [8] S. Gopalakrishnan, B. L. Lev, and P. M. Goldbart, “Frustration and glassiness in spin models with cavity-mediated interactions,” *Phys. Rev. Lett.* **107**, 277201 (2011).
- [9] J. S. Douglas, H. Habibian, C.-L. Hung, A. V. Gorshkov, H. J. Kimble, and D. E. Chang, “Quantum many-body models with cold atoms coupled to photonic crystals,” *Nat. Photonics* **9**, 326 (2015).
- [10] C.-L. Hung, A. González-Tudela, J. I. Cirac, and H. J. Kimble, “Quantum spin dynamics with pairwise-tunable, long-range interactions,” *Proc. Natl. Acad. Sci. U.S.A.* **113**, E4946 (2016).
- [11] J. W. Britton, B. C. Sawyer, A. C. Keith, C.-C. J. Wang, J. K. Freericks, H. Uys, M. J. Biercuk, and J. J. Bollinger, “Engineered two-dimensional Ising interactions in a trapped-ion quantum simulator with hundreds of spins,” *Nature (London)* **484**, 489 (2012).
- [12] P. Richerme, Z.-X. Gong, A. Lee, C. Senko, J. Smith, M. Foss-Feig, S. Michalakis, A. V. Gorshkov, and C. Monroe, “Non-local propagation of correlations in quantum systems with long-range interactions,” *Nature (London)* **511**, 198 (2014).
- [13] P. Jurcevic, B. P. Lanyon, P. Hauke, C. Hempel, P. Zoller, R. Blatt, and C. F. Roos, “Quasiparticle engineering and entanglement propagation in a quantum many-body system,” *Nature (London)* **511**, 202 (2014).
- [14] J. Smith, A. Lee, P. Richerme, B. Neyenhuis, P. W. Hess, P. Hauke, M. Heyl, D. A. Huse, and C. Monroe, “Many-body localization in a quantum simulator with programmable random disorder,” *Nat. Phys.* **12**, 907 (2016).
- [15] J. Zhang, G. Pagano, P. W. Hess, A. Kyprianidis, P. Becker, H. Kaplan, A. V. Gorshkov, Z.-X. Gong, and C. Monroe, “Observation of a many-body dynamical phase transition with a 53-qubit quantum simulator,” *Nature (London)* **551**, 601 (2017).
- [16] K.-K. Ni, S. Ospelkaus, M. H. G. de Miranda, A. Pe’er, B. Neyenhuis, J. J. Zirbel, S. Kotochigova, P. S. Julienne, D. S. Jin, and J. Ye, “A High Phase-Space-Density Gas of Polar Molecules,” *Science* **322**, 231 (2008).
- [17] K.-K. Ni, S. Ospelkaus, D. Wang, G. Quémener, B. Neyenhuis, M. H. G. de Miranda, J. L. Bohn, J. Ye, and D. S. Jin, “Dipolar collisions of polar molecules in the quantum regime,” *Nature (London)* **464**, 1324 (2010).
- [18] A. Chotia, B. Neyenhuis, S. A. Moses, B. Yan, J. P. Covey, M. Foss-Feig, A. M. Rey, D. S. Jin, and J. Ye, “Long-Lived Dipolar Molecules and Feshbach Molecules in a 3D Optical Lattice,” *Phys. Rev. Lett.* **108**, 080405 (2012).
- [19] P. K. Molony, P. D. Gregory, Z. Ji, B. Lu, M. P. Köppinger, C. R. Le Sueur, C. L. Blackley, J. M. Hutson, and S. L. Cornish, “Creation of ultracold  $^{87}\text{Rb}^{133}\text{Cs}$  molecules in the rovibrational ground state,” *Phys. Rev. Lett.* **113**, 255301 (2014).
- [20] K. Aikawa, A. Frisch, M. Mark, S. Baier, A. Rietzler, R. Grimm, and F. Ferlaino, “Bose-einstein condensation of erbium,” *Phys. Rev. Lett.* **108**, 210401 (2012).
- [21] G. Balasubramanian, P. Neumann, D. Twitchen, M. Markham, R. Kolesov, N. Mizuochi, J. Isoya, J. Achard, J. Beck, J. Tissler, V. Jacques, P. R. Hemmer, F. Jelezko, and J. Wrachtrup, “Ultra-long spin coherence time in isotopically engineered diamond,” *Nat. Mater.* **8**, 383 (2009).
- [22] L. Béguin, A. Vernier, R. Chicireanu, T. Lahaye, and A. Browaeys, “Direct measurement of the van der waals interaction between two rydberg atoms,” *Phys. Rev. Lett.* **110**, 263201 (2013).
- [23] Y. O. Dudin and A. Kuzmich, “Strongly Interacting Rydberg Excitations of a Cold Atomic Gas,” *Science* **336**, 887 (2012).
- [24] E. H. Lieb and D. W. Robinson, “The finite group velocity of quantum spin systems,” *Commun. Math. Phys.* **28**, 251–257 (1972).
- [25] Z.-X. Gong, M. Foss-Feig, S. Michalakis, and Alexey V. G., “Persistence of locality in systems with power-law interactions,” *Phys. Rev. Lett.* **113**, 030602 (2014).
- [26] M. Foss-Feig, Z.-X. Gong, C. W. Clark, and A. V. Gorshkov, “Nearly linear light cones in long-range interacting quantum systems,” *Phys. Rev. Lett.* **114**, 157201 (2015).
- [27] P. Hauke and L. Tagliacozzo, “Spread of correlations in long-range interacting quantum systems,” *Phys. Rev. Lett.* **111**, 207202 (2013).

- [28] J. Schachenmayer, B. P. Lanyon, C. F. Roos, and A. J. Daley, “Entanglement growth in quench dynamics with variable range interactions,” *Phys. Rev. X* **3**, 031015 (2013).
- [29] L. Vanderstraeten, M. Van Damme, H. P. Büchler, and F. Verstraete, “Quasiparticles in quantum spin chains with long-range interactions,” [arXiv:1801.00769](https://arxiv.org/abs/1801.00769).
- [30] A. S. Buyskikh, M. Fagotti, J. Schachenmayer, F. Essler, and A. J. Daley, “Entanglement growth and correlation spreading with variable-range interactions in spin and fermionic tunneling models,” *Phys. Rev. A* **93**, 053620 (2016).
- [31] M. B. Hastings and T. Koma, “Spectral Gap and Exponential Decay of Correlations,” *Commun. Math. Phys.* **265**, 781 (2006).
- [32] M. F. Maghrebi, Z.-X. Gong, and A.V. Gorshkov, “Continuous symmetry breaking in 1d long-range interacting quantum systems,” *Phys. Rev. Lett.* **119**, 023001 (2017).
- [33] N. D. Mermin and H. Wagner, “Absence of ferromagnetism or antiferromagnetism in one- or two-dimensional isotropic heisenberg models,” *Phys. Rev. Lett.* **17**, 1133 (1966).
- [34] M. Kormos, M. Collura, G. Takács, and P. Calabrese, “Real-time confinement following a quantum quench to a non-integrable model,” *Nat. Phys.* **13**, 246 (2017).
- [35] J. Greensite, “An introduction to the confinement problem,” *Lect. Notes Phys.* **821**, 1 (2011).
- [36] N. Vandersickel and D. Zwanziger, “The Gribov problem and QCD dynamics,” *Phys. Rep.* **520**, 175 (2012).
- [37] R. Coldea, D. A. Tennant, E. M. Wheeler, E. Wawrzynska, D. Prabhakaran, M. Telling, K. Habicht, P. Smeibidl, and K. Kiefer, “Quantum Criticality in an Ising Chain: Experimental Evidence for Emergent  $E_8$  Symmetry,” *Science* **327**, 177 (2010).
- [38] S. B. Rutkevich, “Energy Spectrum of Bound-Spinons in the Quantum Ising Spin-Chain Ferromagnet,” *J. Stat. Phys.* **131**, 917 (2008).
- [39] C. M. Morris, R. Valdés Aguilar, A. Ghosh, S. M. Koohpayeh, J. Krizan, R. J. Cava, O. Tchernyshyov, T. M. McQueen, and N. P. Armitage, “Hierarchy of bound states in the one-dimensional ferromagnetic ising chain  $\text{conb}_{206}$  investigated by high-resolution time-domain terahertz spectroscopy,” *Phys. Rev. Lett.* **112**, 137403 (2014).
- [40] J. A. Kjäll, F. Pollmann, and J. E. Moore, “Bound states and  $E_8$  symmetry effects in perturbed quantum ising chains,” *Phys. Rev. B* **83**, 020407 (2011).
- [41] G. Delfino, “Quantum quenches with integrable pre-quench dynamics,” *J. Phys. A* **47**, 402001 (2014).
- [42] G. Delfino and J. Viti, “On the theory of quantum quenches in near-critical systems,” *J. Phys. A* **50**, 084004 (2017).
- [43] P. Calabrese, F. H. L. Essler, and M. Fagotti, “Quantum Quench in the Transverse-Field Ising Chain,” *Phys. Rev. Lett.* **106**, 227203 (2011).
- [44] G. Delfino, “Correlation spreading and properties of the quantum state in quench dynamics,” *Phys. Rev. E* **97**, 062138 (2018).
- [45] B. M. McCoy and T. T. Wu, “Two-dimensional ising field theory in a magnetic field: Breakup of the cut in the two-point function,” *Phys. Rev. D* **18**, 1259 (1978).
- [46] B. M. McCoy and T. T. Wu, “Theory of a two-dimensional ising model with random impurities. i. thermodynamics,” *Phys. Rev.* **176**, 631 (1968).
- [47] B. M. McCoy and J.-M. Maillard, “The importance of the ising model,” *Prog. Theor. Phys.* **127**, 791 (2012).
- [48] M. C. Bañuls, J. I. Cirac, and M. B. Hastings, “Strong and weak thermalization of infinite nonintegrable quantum systems,” *Phys. Rev. Lett.* **106**, 050405 (2011).
- [49] C.-J. Lin and O. I. Motrunich, “Quasiparticle explanation of the weak-thermalization regime under quench in a nonintegrable quantum spin chain,” *Phys. Rev. A* **95**, 023621 (2017).
- [50] J. Zhang, P. W. Hess, A. Kyprianidis, P. Becker, A. Lee, J. Smith, G. Pagano, I.-D. Potirniche, A. C. Potter, A. Vishwanath, N. Y. Yao, and C. Monroe, “Observation of a discrete time crystal,” *Nature (London)* **543**, 217 (2017).
- [51] P. W. Hess, P. Becker, H. B. Kaplan, A. Kyprianidis, A. C. Lee, B. Neyenhuis, G. Pagano, P. Richerme, C. Senko, J. Smith, W. L. Tan, J. Zhang, and C. Monroe, “Non-thermalization in trapped atomic ion spin chains,” *Philos. Trans. Royal Soc. A* **375**, 20170107 (2017).
- [52] F. Machado, G. D. Meyer, D. V. Else, C. Nayak, and N. Y. Yao, “Exponentially Slow Heating in Short and Long-range Interacting Floquet Systems,” [arXiv:1708.01620](https://arxiv.org/abs/1708.01620).
- [53] H. Bernien, S. Schwartz, A. Keesling, H. Levine, A. Omran, H. Pichler, S. Choi, A. S. Zibrov, M. Endres, M. Greiner, V. Vuletić, and M. D. Lukin, “Probing many-body dynamics on a 51-atom quantum simulator,” *Nature (London)* **551**, 579 (2017).
- [54] S. Sachdev, *Quantum Phase Transitions*, (Cambridge University Press, Cambridge) (2011).
- [55] T. Koffel, M. Lewenstein, and L. Tagliacozzo, “Entanglement Entropy for the Long-Range Ising Chain in a Transverse Field,” *Phys. Rev. Lett.* **109**, 267203 (2012).
- [56] M. Knap, A. Kantian, T. Giamarchi, I. Bloch, M. D. Lukin, and E. Demler, “Probing real-space and time-resolved correlation functions with many-body Ramsey interferometry,” *Phys. Rev. Lett.* **111**, 147205 (2013).
- [57] S. Fey and K. P. Schmidt, “Critical behavior of quantum magnets with long-range interactions in the thermodynamic limit,” *Phys. Rev. B* **94**, 075156 (2016).
- [58] S. Fey, Sebastian C. Kapfer, and K. P. Schmidt, “Quantum criticality of two-dimensional quantum magnets with long-range interactions,” [arXiv:1802.06684](https://arxiv.org/abs/1802.06684).
- [59] P. Jurcevic, H. Shen, P. Hauke, C. Maier, T. Brydges, C. Hempel, B. P. Lanyon, M. Heyl, R. Blatt, and C. F. Roos, “Direct observation of dynamical quantum phase transitions in an interacting many-body system,” *Phys. Rev. Lett.* **119**, 080501 (2017).
- [60] P. Calabrese and J. Cardy, “Time dependence of correlation functions following a quantum quench,” *Phys. Rev. Lett.* **96**, 136801 (2006).
- [61] D. J. Luitz and Y. B. Lev, “The ergodic side of the many-body localization transition,” *Ann. Phys. (Berlin)* **529**, 1600350 (2017).
- [62] A. Nauts and R. E. Wyatt, “New approach to many-state quantum dynamics: The recursive-residue-generation method,” *Phys. Rev. Lett.* **51**, 2238 (1983).
- [63] See Supplemental Material for detailed numerics of light-cone spreading of the correlations, and discussions on convergent and scaling properties of mesonic masses.
- [64] For Fig. 2(b), we use parameters and probing time relevant to current trapped-ion experiments [12, 13, 15].
- [65] V. Zauner-Stauber and J. C. Halimeh, “Probing the anomalous dynamical phase in long-range quantum spin chains through fisher-zero lines,” *Phys. Rev. E* **96**, 062118 (2017).
- [66] J. C. Halimeh, V. Zauner-Stauber, I. P. McCulloch, I. de Vega, U. Schollwöck, and M. Kastner, “Prethermalization and persistent order in the absence of a thermal phase transition,” *Phys. Rev. B* **95**, 024302 (2017).
- [67] J. C. Halimeh and V. Zauner-Stauber, “Dynamical phase diagram of quantum spin chains with long-range interactions,” *Phys. Rev. B* **96**, 134427 (2017).
- [68] The time step used in Fig. 2 is 0.05.
- [69] S. B. Rutkevich, “On the weak confinement of kinks in the one-

- dimensional quantum ferromagnet  $\text{CoNb}_2\text{O}_6$ ,” *J. Stat. Mech. Theory Exp.* **7**, 07015 (2010).
- [70] The energy difference between (bounded) excited states at  $k = 0$  and the ground state.
- [71] E. C. Titchmarsh and D. R. Heath-Brown, *The theory of the Riemann zeta-function*, (Oxford University Press, Oxford) (1986).
- [72] L. F. Santos, F. Borgonovi, and G. L. Celardo, “Cooperative Shielding in Many-Body Systems with Long-Range Interaction,” *Phys. Rev. Lett.* **116**, 250402 (2016).
- [73] A. J. A. James, R. M. Konik, and N. J. Robinson, “Nonthermal states arising from confinement in one and two dimensions,” [arXiv:1804.09990](https://arxiv.org/abs/1804.09990).
- [74] P. P. Mazza, G. Peretto, A. Lerose, M. Collura, and A. Gambassi, “Suppression of transport in non-disordered quantum spin chains due to confined excitations,” [arXiv:1806.09674](https://arxiv.org/abs/1806.09674).
- [75] T. Rakovszky, M. Mestyán, M. Collura, M. Kormos, and G. Takács, “Hamiltonian truncation approach to quenches in the Ising field theory,” *Nucl. Phys. B* **911**, 805 (2016).
- [76] N. J. Robinson, A. J. A. James, and R. M. Konik, “Signatures of rare states and thermalization in a theory with confinement,” [arXiv:1808.10782](https://arxiv.org/abs/1808.10782).
- [77] J. R. Garrison and T. Grover, “Does a single eigenstate encode the full hamiltonian?” *Phys. Rev. X* **8**, 021026 (2018).
- [78] I.-D. Potirniche, A. C. Potter, M. Schleier-Smith, A. Vishwanath, and N. Y. Yao, “Floquet Symmetry-Protected Topological Phases in Cold-Atom Systems,” *Phys. Rev. Lett.* **119**, 123601 (2017).
- [79] C. W. von Keyserlingk and S. L. Sondhi, “Phase structure of one-dimensional interacting floquet systems. i. abelian symmetry-protected topological phases,” *Phys. Rev. B* **93**, 245145 (2016).
- [80] C. W. von Keyserlingk and S. L. Sondhi, “Phase structure of one-dimensional interacting floquet systems. ii. symmetry-broken phases,” *Phys. Rev. B* **93**, 245146 (2016).
- [81] A. C. Potter, T. Morimoto, and A. Vishwanath, “Classification of interacting topological floquet phases in one dimension,” *Phys. Rev. X* **6**, 041001 (2016).
- [82] D. V. Else and C. Nayak, “Classification of topological phases in periodically driven interacting systems,” *Phys. Rev. B* **93**, 201103 (2016).
- [83] G. Delfino and P. Grinza, “Confinement in the q-state Potts field theory,” *Nucl. Phys. B* **791**, 265 (2008).
- [84] L. Lepori, G. Z. Tóth, and G. Delfino, “The particle spectrum of the three-state Potts field theory: a numerical study,” *J. Stat. Mech. Theory Exp.* **2009**, 11007 (2009).
- [85] S. B. Rutkevich, “Baryon masses in the three-state Potts field theory in a weak magnetic field,” *J. Stat. Mech. Theory Exp.* **1**, 01010 (2015).
- [86] M. Lencsés and G. Takács, “Confinement in the q-state Potts model: an RG-TCSA study,” *J. High Energy Phys.* **9**, 146 (2015).

## Supplemental Material

This Supplemental Material is organized as follows. In Sec. I, we provide detailed numerical results showing light-cone spreading of correlation functions by zooming in on Figs. 1 (b) and (c) in the main text. In Sec. II, we provide a detailed analysis on the scaling and convergence of the potential in the main text.

### I. LIGHT-CONE SPREADING OF CORRELATION FUNCTIONS

In the main text, we have shown that the magnitude of  $\langle \sigma_j^z(t) \sigma_k^z(t) \rangle_c$  is suppressed by long-range interactions. As stressed in the main text, this does not indicate the disappearance of the light-cone spreading of correlations (quantum information). In this section, we provide detailed numerics showing that the light-cone behaviour is still present by zooming in on the weak-signal regions of Figs. 1(b) and (c) of the main text.

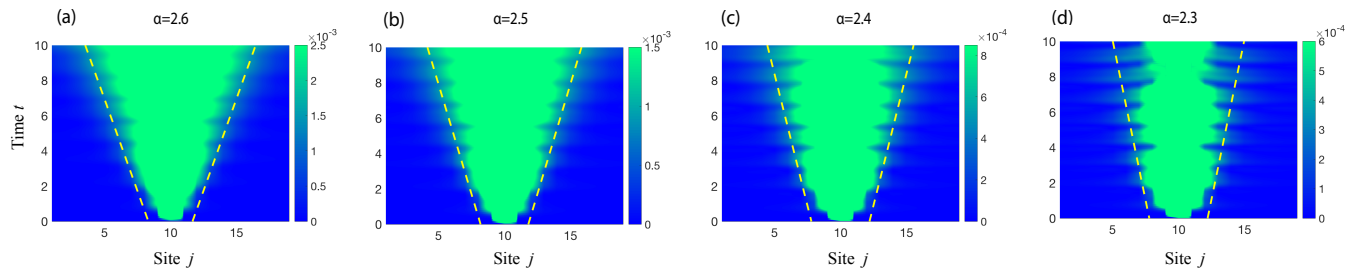


FIG. S1. (color online)  $\langle \sigma_j^z \sigma_k^z \rangle_c$  after a quantum quench with initial state  $|\Psi_0\rangle$ . Parameters:  $L = 19$ ,  $k = 10$ , and  $B = 0.27$ . (a)  $\alpha = 2.6$ , (b)  $\alpha = 2.5$ , (c)  $\alpha = 2.4$ , (d)  $\alpha = 2.3$ . The green regions represent out-of-range values of the correlation functions. The yellow dashed lines illustrate twice the maximal velocity of quasiparticles (within the three lowest energy bands). The maximal velocity for each  $\alpha$  is calculated using the two-kink model, and takes the value of  $v_{max} = 0.24J$ ,  $0.20J$ ,  $0.17J$ ,  $0.14J$  for (a), (b), (c), and (d), respectively. The speed at which the front of the time-dependent correlation function propagates is consistent with twice the maximal velocity of the quasiparticles.

Figs. S1(a)-(d) show correlation spreading after a sudden quench (for the same initial state,  $|\Psi_0\rangle$ ), as in the main text) for several different  $\alpha$ . Figs. S1 (a) and (d) take the same parameters of the post-quench Hamiltonians as Figs. 1 (b) and (c) in the main text, but use an intensity scale up to two orders magnitude smaller. By zooming in on the weak-signal regions, we observe that correlations do indeed exhibit light-cone spreading, though they may spread at different maximal velocities compared to the short-range case. These results are consistent with the general theory of quench dynamics in one-dimensional systems first formulated in Refs. [41, 42] for short-range interacting systems, where the light-cone spreading of correlations is always present with a slope equal to twice the maximal velocity of the quasiparticles.

### II. SCALING AND CONVERGENCE ANALYSIS OF CONFINING POTENTIAL

In this section, we provide a detailed analysis on the scaling and convergence of the potential that appears in the two-kink model. We use integrals to approximate sums. While this does not give an exact value for the potential, we will see that scaling exponents given by this approximation agree well with numerics presented in the main text.

We use  $V(n, L, \alpha)$  to denote the potential energy of a two-domain-wall state with length  $n$  on a finite chain of length  $L$ . The potential can be rewritten in the following form:

$$V(n, L, \alpha) = 4 \left[ \sum_{r=1}^L \frac{1}{r^\alpha} + \sum_{r=2}^L \frac{1}{r^\alpha} + \dots + \sum_{r=n}^L \frac{1}{r^\alpha} - 1 \right]. \quad (\text{S1})$$

Note that Eq. (4) in the main text can be obtained by taking the above equation to the thermodynamic limit.

We now approximate the above sums with integrals, which gives

$$\tilde{V}(n, L, \alpha) = 4 \left[ \int_1^L \frac{1}{r^\alpha} dr + \int_2^L \frac{1}{r^\alpha} dr + \dots + \int_n^L \frac{1}{r^\alpha} dr - 1 \right] = 4 \left[ \frac{1}{\alpha-1} \left( \sum_{r=1}^n \frac{1}{r^{\alpha-1}} - \frac{n}{L^{\alpha-1}} \right) - 1 \right]. \quad (\text{S2})$$



After approximating the remaining sum, we obtain

$$\tilde{V}(n, L, \alpha) = 4 \left[ \frac{1}{\alpha - 1} \left( \int_1^n \frac{1}{r^{\alpha-1}} dr - \frac{n}{L^{\alpha-1}} \right) - 1 \right] = 4 \left[ \frac{1 - 1/n^{\alpha-2}}{(\alpha - 1)(\alpha - 2)} - \frac{n}{(\alpha - 1)L^{\alpha-1}} - 1 \right]. \quad (\text{S3})$$

Three comments are in order: (i) The second term in the above expression tells us that, for finite  $n$ , the potential is finite in the thermodynamic limit ( $L \rightarrow \infty$ ) only when  $\alpha > 1$ . Therefore, the masses of these bound states are finite when  $\alpha > 1$ . This agrees with the convergence properties of the Riemann zeta function. (ii) For a finite system, the potential  $\tilde{V}(n, L, \alpha)$  scales as  $c_0 - c_1/L^{\alpha-1}$ . Since all the potential energies of the two-domain-wall states have such scaling, the masses given by eigenenergies of Eq. (3) in the main text should also have the same scaling. This implies that  $\beta$  (defined in the caption to Fig. 3 of the main text) is equal to  $\alpha - 1$ , which is in agreement with the numerical results presented in the inset of Fig. 3(d). (iii) Because of the first term of the above equation,  $V(n)$  goes to infinity when  $n$  goes to infinity for  $1 < \alpha \leq 2$ , while it is upper-bounded when  $\alpha > 2$ . This is also reflected in Fig. 3(a) of the main text. Therefore, when  $\alpha > 2$ , the two-kink model predicts that only the lower part of the energy spectrum is composed of bound states. In other words, for a high enough energy, we have a continuum of states. However, for  $\alpha \leq 2$ , all eigenstates of the two-kink model are bound quasiparticles.